Article ID: 1000-7032(2023)12-2168-12

Luminescence Properties and Energy Transfer of $Ca_{9.15}La_{0.9}(PO_4)_7:Eu^{2+}, Mn^{2+}$ for White LEDs

WANG Tao[1*], ZHANG Xiaoshuai[2], LI Xiaotong[2], WANG Zhijun[2], LI Panlai[2*]

(1. *College of Science, China University of Petroleum (East China), Qingdao* 266580, *China*;
2. *College of Physics Science & Technology, Hebei University, Baoding* 071002, *China*)

* *Corresponding Authors, E-mail: twang@upc. edu. cn; li_panlai@126. com*

Abstract: A series of $Ca_{9.15}La_{0.9}(PO_4)_7:0.05Eu^{2+},yMn^{2+}$ and $Ca_{9.3}La_{0.8}(PO_4)_7:0.05Eu^{2+},yMn^{2+}$ were synthesized by the high temperature solid-state method. The energy transfer from Eu^{2+} to Mn^{2+} was confirmed by the emission spectra and fluorescence decay curves. With increasing the concentration of Mn^{2+}, the phosphor can produce the tuning emission from blue or green to white light. In addition, the thermal stability of the samples revealed that the two emission peaks of Eu^{2+} with different colors exhibited different temperature quenching behaviors. The color coordinates of $Ca_{9.15}La_{0.9}(PO_4)_7:0.05Eu^{2+},0.35Mn^{2+}$ are close to standard white light and the color temperature is similar to sunlight, which proves its potential application in white light emitting diodes (LEDs).

Key words: phosphor; luminescence; energy transfer; $Ca_{9.15}La_{0.9}(PO_4)_7:0.05Eu^{2+},yMn^{2+}$

CLC number: O614; O482.31 **Document code**: A **DOI**: 10.37188/CJL.20230208

白光 LEDs 用 $Ca_{9.15}La_{0.9}(PO_4)_7:Eu^{2+}, Mn^{2+}$ 材料的发光特性及能量传递

王 涛[1*], 张晓帅[2], 李晓彤[2], 王志军[2], 李盼来[2*]

(1. 中国石油大学(华东)理学院, 山东 青岛 266580; 2. 河北大学 物理科学与技术学院, 河北 保定 071002)

摘要: 利用高温固相法合成了 $Ca_{9.15}La_{0.9}(PO_4)_7:0.05Eu^{2+},yMn^{2+}$ 和 $Ca_{9.3}La_{0.8}(PO_4)_7:0.05Eu^{2+},yMn^{2+}$ 系列荧光粉。通过荧光粉的发射光谱和荧光衰减曲线证实 Eu^{2+}、Mn^{2+} 之间存在能量传递,且增大 Mn^{2+} 的掺杂浓度,获得了从青光(绿光)到白光变化的荧光粉。材料的热稳定性显示 Eu^{2+} 的两个不同颜色的发射峰表现出不同的温度猝灭行为。$Ca_{9.15}La_{0.9}(PO_4)_7:0.05Eu^{2+},0.35Mn^{2+}$ 的色坐标接近标准白光且色温与太阳光相近,光谱覆盖整个可见光区域。研究结果表明,材料在白光发光二极管方面有潜在的应用价值。

关 键 词: 发光; 荧光粉; 能量传递; $Ca_{9.15}La_{0.9}(PO_4)_7:0.05Eu^{2+},yMn^{2+}$

1 Introduction

In recent years, the concept of high-quality and healthy lighting has been deeply rooted in the hearts of the people. Full-spectrum phosphors have become a research hotspot in the field of lighting[1-2]. In order to obtain full-spectrum phosphors, it is a simple and effective method to use energy transfer between different ions[3]. The energy transfer from the sensitizer to the activator can not only broaden the

收稿日期: 2023-09-14; **修订日期**: 2023-09-28
基金项目: 国家自然科学基金(61805285)
Supported by National Natural Science Foundation of China(61805285)

emission spectrum coverage of the phosphor, but also continuously regulate the emission color of the phosphor[4]. Compared with the luminescent material doped with a single activator, the luminescent material co-doped with multiple rare earth ions has richer luminescent properties due to its multiple luminescent centers. For example, for $La_2MgGeO_6:Eu^{3+}$, Bi^{3+}, the energy transfer between the two activators is used to change the content of Eu^{3+}, and the regulation of the luminous color from blue to red is realized[5]; for $Ba_{10}(PO_4)_6O:Eu^{2+},Mn^{2+}$, not only realized the change of luminous color from blue to yellow, but also obtained a white light material with broadband emission[6]; for $Sr_6Ca_4(PO_4)_6F_2:Eu^{2+},Mn^{2+}$, when single-doped, there is only a blue light at 450 nm in the emission spectrum, and a red light at 570 nm is added after the introduction of Mn^{2+}, Eu^{2+} can transfer energy to Mn^{2+}. When the content of Mn^{2+} is increased, the emission color can be adjusted, and a white phosphor with broadband emission is obtained[7].

Commonly used red light emitting activators usually choose Sm^{3+}, Pr^{3+}, Mn^{2+}. The former two, because their transition mode is f-f transition, usually exhibit linear emission and cover a small area in the spectrum[8-10]. However, in the research of this paper, it is necessary to obtain a wider spectral coverage as much as possible, hence these two ions are not suitable for use as co-doped activators. In comparison, the transition metal ion Mn^{2+}, which has an unfilled outer electron shell, can generally exhibit broadband emission due to the transition of $^4T_1(4G)\rightarrow{}^6A_1(6S)$, and its 3d energy level is exposed, therefore, with the change of the crystal field, the low-coordination green emission can be transformed into the high-coordination red emission[11]. It is known from previous research reports that the optimal doping concentration of Eu^{2+} is 0.05, so we conducted follow-up experiments on this basis[12]. The matrix can provide a high coordination site for Mn^{2+}, hence series of $Ca_{9.15}La_{0.9}(PO_4)_7:0.05Eu^{2+},yMn^{2+}$ ($C_9L_{0.9}C_{0.15}P:0.05Eu^{2+},yMn^{2+}$) and $Ca_{9.3}La_{0.8}(PO_4)_7:0.05Eu^{2+},yMn^{2+}$ ($C_9L_{0.8}C_{0.3}P:0.05Eu^{2+},yMn^{2+}$) were synthesized, and its luminescent properties were studied.

2　Sample Preparation

2.1　Material Synthesis

The phosphors of $C_9L_{0.9}C_{0.15}P:0.05Eu^{2+},yMn^{2+}$ and $C_9L_{0.8}C_{0.3}P:0.05Eu^{2+},yMn^{2+}$ were synthesized by the high temperature solid state method. The raw materials are $CaCO_3$(99.9%), La_2O_3(99.9%), $MnCO_3$(99.9%), Eu_2O_3(99.9%) and $NH_4H_2PO_4$(99.9%). According to the designed chemical formula composition and stoichiometric ratio (within the allowable error of 0.000 5 g), the required raw materials were calculated and weighed. Grind it in an agate mortar for at least 25 minutes to mix well, and then, all the powders were loaded into an alumina crucible, and placed in a box-type high-temperature furnace for continuous calcination at 1 200 ℃ for 5 hours under a carbon-reducing atmosphere. The carbon-reducing atmosphere would reduce Eu^{3+} to Eu^{2+}. After cooling down naturally, the sample was taken out and placed in a mortar and ground into powder again.

2.2　Material Characterization

The crystal phase of the sample was tested by Bruker D8 X-ray diffractometer, whose radiation source was Cu target Kα (λ=0.154 06 nm), working voltage was 40 kV, working current was 40 mA, scanning range was 2θ =10°−80°, and step size was 0.02 (°)/s, and determine whether the synthesized material is pure phase. The spectral characteristics of the samples were measured by a Hitachi F-4600 fluorescence spectrometer with an excitation source of 450 W xenon lamp, a scanning range of 200−800 nm, a scanning speed of 240 nm/min, and a temperature range of 4−350 K. We use HoribaFL3 to characterize the life decay curve of the sample, use 350 nm nano-LED as the excitation source when testing the life of Eu^{2+}, and use 450 W Xe lamp as the excitation source to test the life of Mn^{2+}.

3　Results and Discussion

3.1　Phase Formation of Samples

Fig. 1(a) shows the XRD patterns of $C_9L_{0.9}C_{0.15}P:0.05Eu^{2+}$, $C_9L_{0.9}C_{0.15}P:0.05Eu^{2+},0.6Mn^{2+}$, $C_9L_{0.8}C_{0.3}P:0.05Eu^{2+}$ and $C_9L_{0.8}C_{0.3}P:0.05Eu^{2+},0.6Mn^{2+}$, and the maximum concentration is selected as a

representative and compared with the standard card (ICSD#59590). It can be seen from the figure that the diffraction peaks of the samples match well with the standard card, and no redundant diffraction peaks appear. It shows that the introduction of Mn^{2+} does not change the crystal structure, and the synthesized sample is a pure phase. In order to further prove that the samples meet the experimental requirements, the refined software GSAS was used to refine the structure of the selected samples, and the

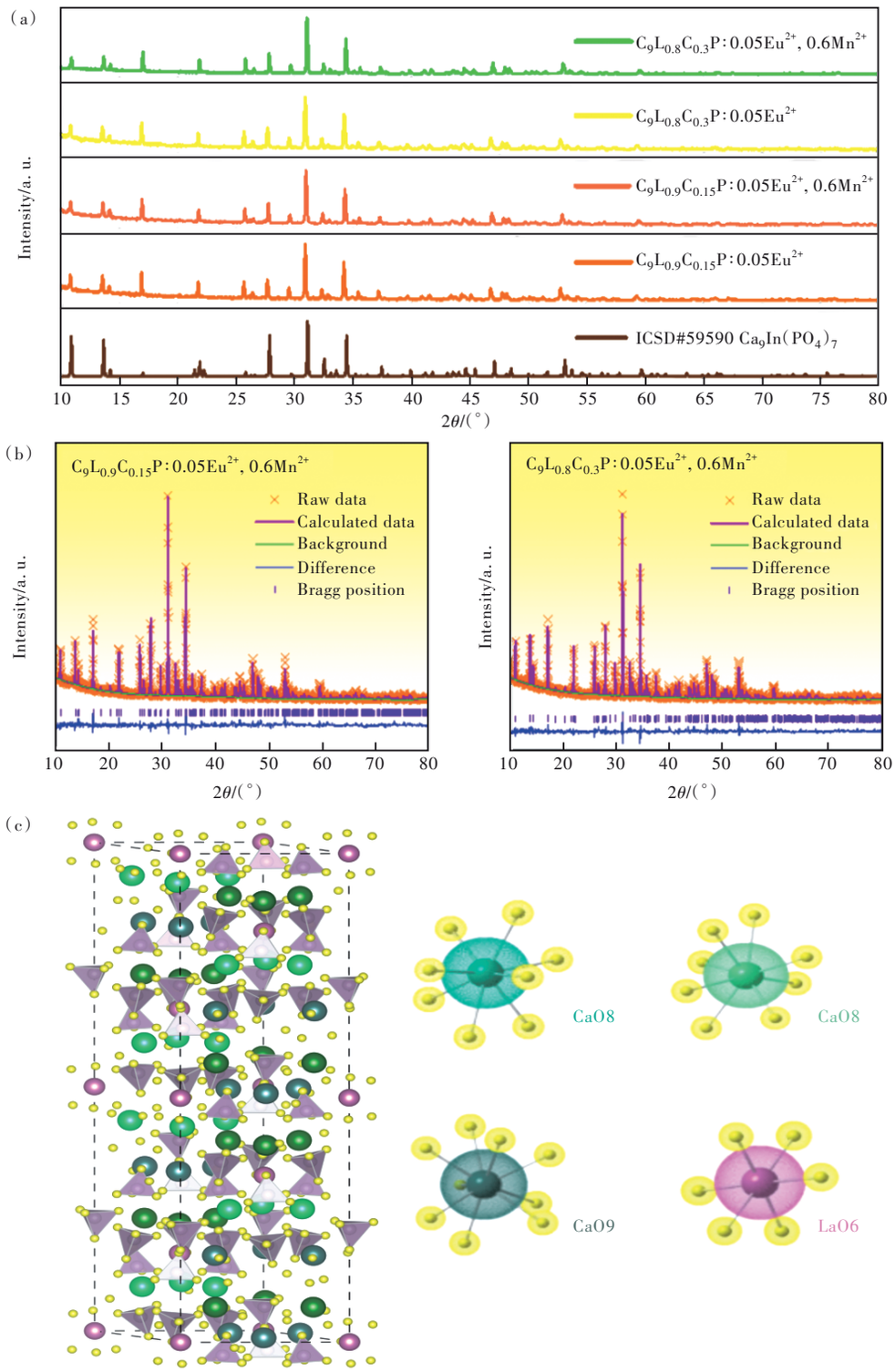

Fig.1 (a) XRD patterns of CLCP: Eu^{2+}, Mn^{2+}. (b) Refinement results of $C_9L_{0.9}C_{0.15}P:0.05Eu^{2+}, 0.6Mn^{2+}$ and $C_9L_{0.8}C_{0.3}P:0.05Eu^{2+}, 0.6Mn^{2+}$ based on ICSD#59590 standard card. (c) Crystal structure of $Ca_9La(PO_4)_7$.

results are shown in Fig. 1(b). The specific refinement parameters can be seen from the attached Tab. S1, both R_p and R_{wp} meet the experimental requirements (less than 10% and 15% respectively). And the unit cell volume V decreases in different degrees. It is proved that the transition metal Mn^{2+} can be successfully introduced into the matrix without changing the structure. Fig. 1(c) shows the rich cationic sites present in the matrix. Depending on the match between the valence state and the radius of the ion, Eu^{2+} and Mn^{2+} will randomly replace three different calcium positions.

3.2 Luminescence Properties

Fig. 2(a) and (b) depict the emission spectra of $C_9L_{0.9}C_{0.15}P$: 0.05Eu^{2+}, $y$$Mn^{2+}$ and $C_9L_{0.8}C_{0.3}P$: 0.05Eu^{2+}, $y$$Mn^{2+}$ under 330 nm excitation. And the spectrum exhibits a broad coverage range from 380 nm to 750 nm, and the three emission bands located art 427, 510, 650 nm, respectively. With the increase of the Mn^{2+} concentrations, the intensities of the first two emission peaks are continuously weakened, and the intensity of the latter emission peak is continuously enhanced. At y = 0.6, the intensity of the emission peak reaches the maximum, and then begins to weakened. As shown in Fig. S1, under 330 nm excitation, the emission spectra of $C_9L_{0.8}C_{0.3}P$: Eu^{2+}, C_9L_1P: Eu^{2+} and the excitation spectra corresponding to the two emission peaks were tested, and the two emission peaks were located at around 427 nm and 510 nm, respectively. Fig. 2(a)-(b) and Fig. S1 show that the first two peaks come from the luminescence of Eu^{2+} ions in different lattice positions, hence it is obvious that the emission peak at 650 nm belongs to Mn^{2+}, which is very similar to the results in the literature[12]. The illustration shows the effect of the change of Mn^{2+} doping concentration on the luminescence of the three emission peaks. The change of emission intensity in the figure implies that there may be the energy transfer between Eu^{2+} and Mn^{2+} in the sample, indicating that the regulation of the matrix has no effect on the fact that the energy transfer between the two may occur. The

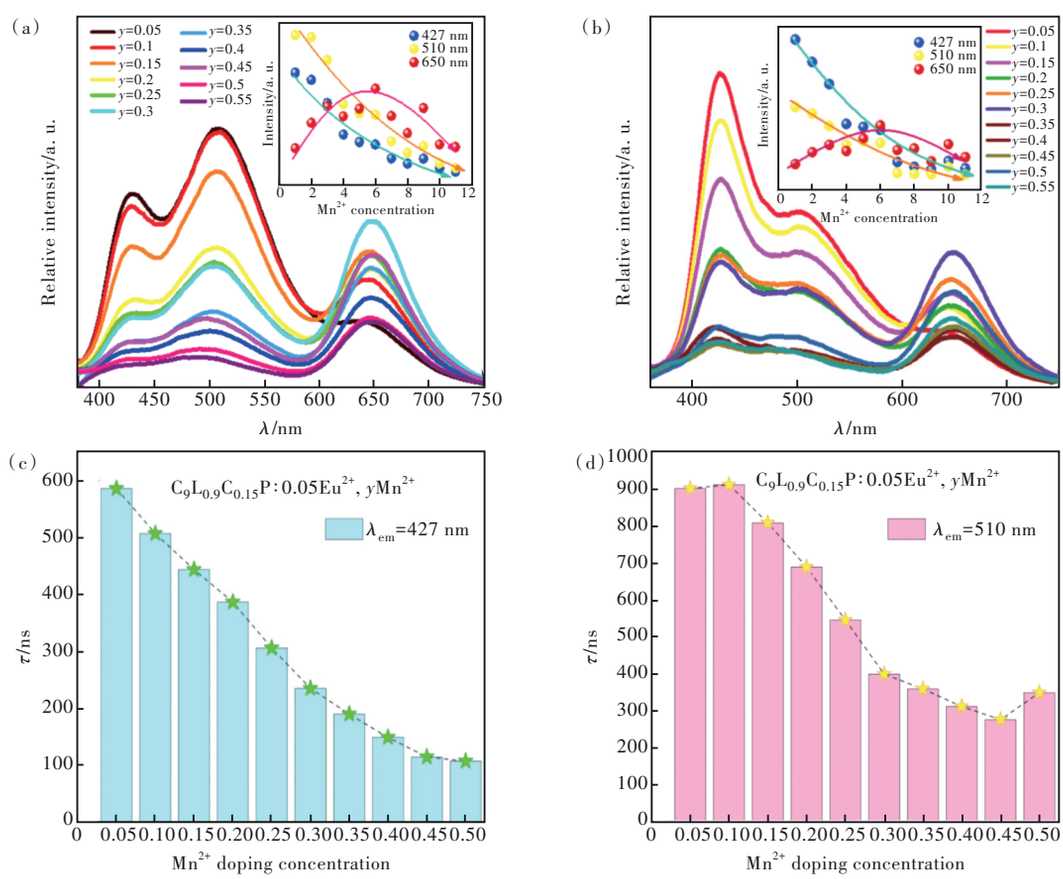

Fig.2 Emission spectra of $C_9L_{0.9}C_{0.15}P$: 0.05Eu^{2+}, $y$$Mn^{2+}$ (a) and $C_9L_{0.8}C_{0.3}P$: 0.05Eu^{2+}, $y$$Mn^{2+}$ (b) (λ_{ex}=330 nm). Lifetime of Eu^{2+} in $C_9L_{0.9}C_{0.15}P$: 0.05Eu^{2+}, $y$$Mn^{2+}$ (λ_{em}=427 nm) (c) and (λ_{em}=510 nm) (d).

regulation of matrix components only affects the energy transfer efficiency between Eu^{2+} and Mn^{2+}.

In order to verify whether there is energy transfer between Eu^{2+} and Mn^{2+} in CLCP: $0.05Eu^{2+}$, yMn^{2+}, $C_9L_{0.9}C_{0.15}P$ is used as an example. We monitor the fluorescence curves of Eu^{2+} ions at 427 nm and 510 nm, respectively, and the results are shown in Fig. S2. According to the equations (1) and (2)[13-15]:

$$I = I_0 + A_1 \exp(-t/\tau_1) + A_2 \exp(-t/\tau_2), \quad (1)$$

where $I(t)$ represent the luminous intensity, A_1 and A_2 are constants, t is time, and τ_1 and τ_2 are the fast and slow decay lifetime. The average effective lifetime of an ion can be calculated as:

$$\tau^* = (A_1\tau_1^2 + A_2\tau_2^2)/(A_1\tau_1 + A_2\tau_2), \quad (2)$$

the results obtained by the formula are recorded in Tab. S2, and the results are shown in Fig. 2(c)-(d). With increasing the Mn^{2+} concentration, the lifetime of the two Eu^{2+} peaks tends to decrease. The lifetime obtained at 427 nm attenuates from 587.3 ns to 49.4 ns, and the lifetime obtained at 510 nm attenuates from 903.7 ns to 237.6 ns. Obviously, the energy transfer from Eu^{2+} to Mn^{2+} exists in $C_9L_{0.9}C_{0.15}P$: $0.05Eu^{2+}$,yMn^{2+}. The energy transfer efficiency(η_T) can be calculated by equation (3)[16]:

$$\eta_T = 1-(I_S/I_{S0}), \quad (3)$$

I_S and I_{S0} are the luminous intensities of the sensitizer Eu^{2+} incorporated with the activator Mn^{2+} and the unincorporated activator Mn^{2+}, respectively. The energy transfer efficiency of $Eu^{2+}\rightarrow Mn^{2+}$ in $C_9L_{0.9}C_{0.15}P$: $0.05Eu^{2+}$, yMn^{2+} is calculated as shown in Tab. S3. The concentration of Eu^{2+} is fixed, the energy transfer efficiency of $Eu^{2+}\rightarrow Mn^{2+}$ increases with the concentration of Mn^{2+} increasing, and when $x = 0.6$, the energy transfer efficiencies reach the maximum 91.9% and 94.1%, respectively. In general, the energy transfer between ions mainly has two mechanisms: exchange interaction and multipolar interaction[17]. The judgment of what is dominant between the two is based on the magnitude of the critical distance(R_C). When the critical distance is less than 0.5 nm, the exchange interaction dominates. Conversely, when the critical distance is greater than 0.5 nm, the multipolar interactions predominate[18]. The distance between the activator and the sensitizer will gradually decrease with the increase of the concentration of the activator, and when the concentration reaches a certain value, there will be a significant concentration quenching. In order to study the energy transfer mechanism between Eu^{2+} and Mn^{2+}, the critical distance was calculated by equation (4)[19]:

$$R_C = 2\left[\frac{3V}{4\pi\chi_C N}\right]^{\frac{1}{3}}, \quad (4)$$

where χ_C is the sum of the concentrations of sensitizer and activator, V represents the volume of unit cells, and N is the number of cation lattices that can be replaced by doped ions. For CLCP: $0.05Eu^{2+}$, yMn^{2+}, the unit cell volume is $V = 3.572$ nm^3. The quenching concentration of the activator Mn^{2+} is 0.3. The critical distance calculated by the formula is 1.759 nm, which is significantly greater than the maximum critical distance of 0.5 nm[20-21]. Therefore, the energy transfer mechanism is the multipolar interaction.

To further identify the energy transfer mechanism, the formula (5)[22] can be obtained based on Dexter's energy transfer theory[23] and Reisfeld's approximation[24]:

$$\frac{\eta_{S0}}{\eta_S} \propto C_{Ln^{2+}}^{n/3}, \quad (5)$$

η_{S0} and η represent the luminescent efficiency of the sensitizer Eu^{2+} ion when it is not introduced and after introduction, C is the sum of the concentration of sensitizer and activator, Ln^{2+} represents Mn^{2+}, and when the n values are 6, 8 and 10, they correspond to dipole-dipole, dipole-quadrupole and quadrupole-quadrupole interactions, respectively. Usually, the quantum efficiency ratio required in the formula in the actual test is difficult to obtain, hence the ratio of peaks and strengths (I_{S0}/I_S) in the emission spectra can be approximated to obtain the equation[25-26]:

$$\frac{I_{S0}}{I_S} \propto C_{Ln^{2+}}^{n/3}, \quad (6)$$

I_S and I_{S0} indicate the luminous intensity of Eu^{2+} ions with or without Mn^{2+}, respectively. Fig. 3(a) shows the results obtained after fitting, respectively, n takes 6, 8, 10, which corresponds to the dipole-

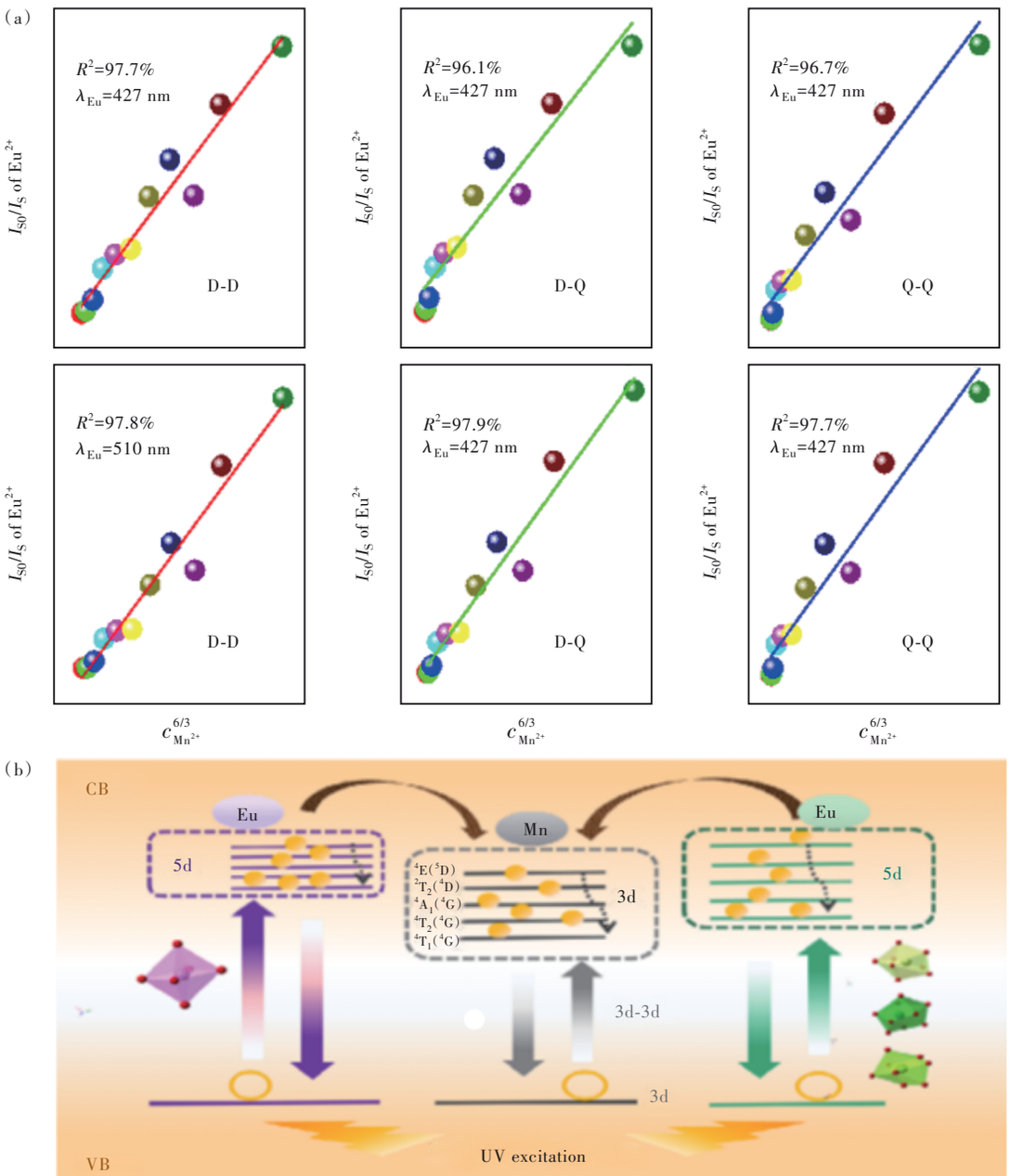

Fig. 3　(a) The relationship between I_{S0}/I_S and content. (b) Energy transfer process and energy level model of Eu^{2+} and Mn^{2+} in CLCP.

dipole, dipole-quadrupole and quadrupole-quadrupole interactions, respectively. Obviously, the energy transfer mechanism is a dipole-dipole interaction.

In CLCP, the energy level model between the two ions is shown in Fig. 3(b), the outermost electrons of the Eu^{2+} ion are sensitive to the crystal field environment, and the 5d energy levels in different environments show different degrees of cleavage, resulting in emission wavelengths of different sizes. Similarly, the 3d energy level of Mn^{2+} ions will also be affected by the crystal field and the energy level will split, and the energy levels after splitting are ^4E (4D), $^2T_2$ (4D), $^4A_1$ (4G), $^4T_2$ (4G) and $^4T^1$ (4G). Eu^{2+} in different grids can simultaneously transfer energy to the 3d level of Mn^{2+}. And changing the matrix does not affect the luminescence of Mn^{2+} ions, and still shows broadband red light emission.

3.3　Temperature Properties and Color Coordinates

Considering that the temperature of phosphors rises when applied to LEDs, we selected the most optimal temperature properties of the sample material

when y = 0.35. The material gradually warmed up from 298 K to 448 K, and in order to make the data as accurate as possible, the test was carried out after 3 minutes at each test temperature point, and the results obtained were shown in Fig. 4(a). It is clear from Fig. 4(b) that the three emission peaks are clearly different. Among them, the emission intensity of Mn^{2+} ions at 650 nm decreased the fastest, and the emission intensity of Eu^{2+} ions at 510 nm decreased at the second rate. The emission at 427 nm, which also belongs to Eu^{2+}, has little change in intensity during the warming process. The ratio of the intensity measured at each temperature to the initial intensity is calculated and shown in Fig. 4(c). Among them, for LED chips, 423 K is usually the highest temperature when it is operating. The intensity of the three emission peaks at this time is 96.1%, 46.6% and 29.4% from shortwave to longwave relative to 298 K. As the temperature increases, the emission intensities change, and the corresponding color coordinates also change. As can be seen from Fig. 4(d), the color coordinates of the sample gradually shift from the low color temperature part to the high color temperature part during the heating process, but remain in the white light range.

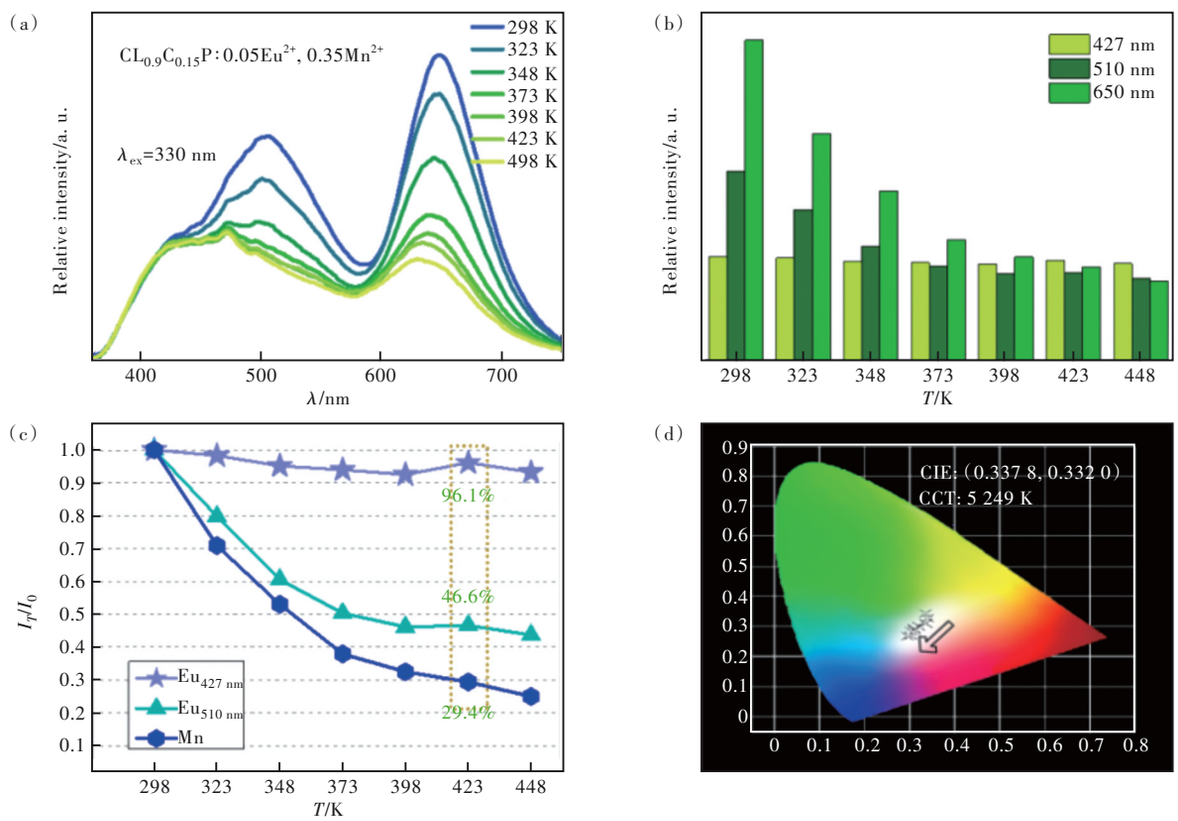

Fig.4 (a)Temperature properties of CLCP:$0.05Eu^{2+}$,$0.35Mn^{2+}$. (b)Emission intensity as a function of temperature. (c)The ratio (I_T/I_0) at each temperature. (d)Color coordinates with temperature.

Through the test results, it was found that the same matrix was also Eu^{2+}, but showed different temperature quenching behavior at different cells, which we explored. From numerous literatures, temperature quenching usually consists of two mechanisms, one called thermal ionization and the other thermal activation. Thermal ionization refers to the fact that electrons at the 5d excited state energy level are directly reached by the valence band by the action of heat, and electron transfer occurs without returning to the ground state by transition, hence thermal quenching occurs . Thermal activation is when electrons at the 5d excited state level intensify thermal vibration during heating, cross the barrier, and return to the ground state in the form of radiation-free transitions[27]. For the sample studied herein, as shown in Fig. 5(a), when the Eu^{2+} ions are in different lattices, their 5d energy levels are positioned

differently relative to the bottom of the conduction band. Eu^{2+} ions in coordination 6 have higher energy emission than Eu^{2+} in coordination 7, 8, 9, and their 5d energy levels are closer to the bottom of the conduction band. If the thermal quenching effect is due to thermal ionization, then the shortwave emission Eu^{2+} should be more prone to thermal quenching due to its closer distance to the bottom of the valence band. In practice, the measured data is quite the opposite. Therefore, we consider that the thermal quenching effect of the sample occurs due to the phenomenon of thermal activation. Fig. 5(b) is a schematic diagram of the configuration diagram, and the relationship can be better understood by using the configuration diagram. The relevant parameters are indicated in the figure. Where R is the displacement between the central axis of the ground state and the excited state parabola, E_{zp} is the energy difference between the ground state and the lowest point of the excited state parabola, k is the mechanical constant, and when k increases, the parabola narrows.

Blasse has summarized that in a configuration diagram, when k values are the same, three parameters will affect the thermal stability. The three parameters are R, E_{zp}, $h\nu$[28]. Changing any of these quantities, increasing E_{zp} or decreasing R will increase the barrier at which the radiation-free process occurs, reducing the occurrence of the radiation-free process, thereby showing high thermal stability. In order to clarify the difference between the two emission peaks, using these parameters, several possible scenarios are made under the premise of satisfying

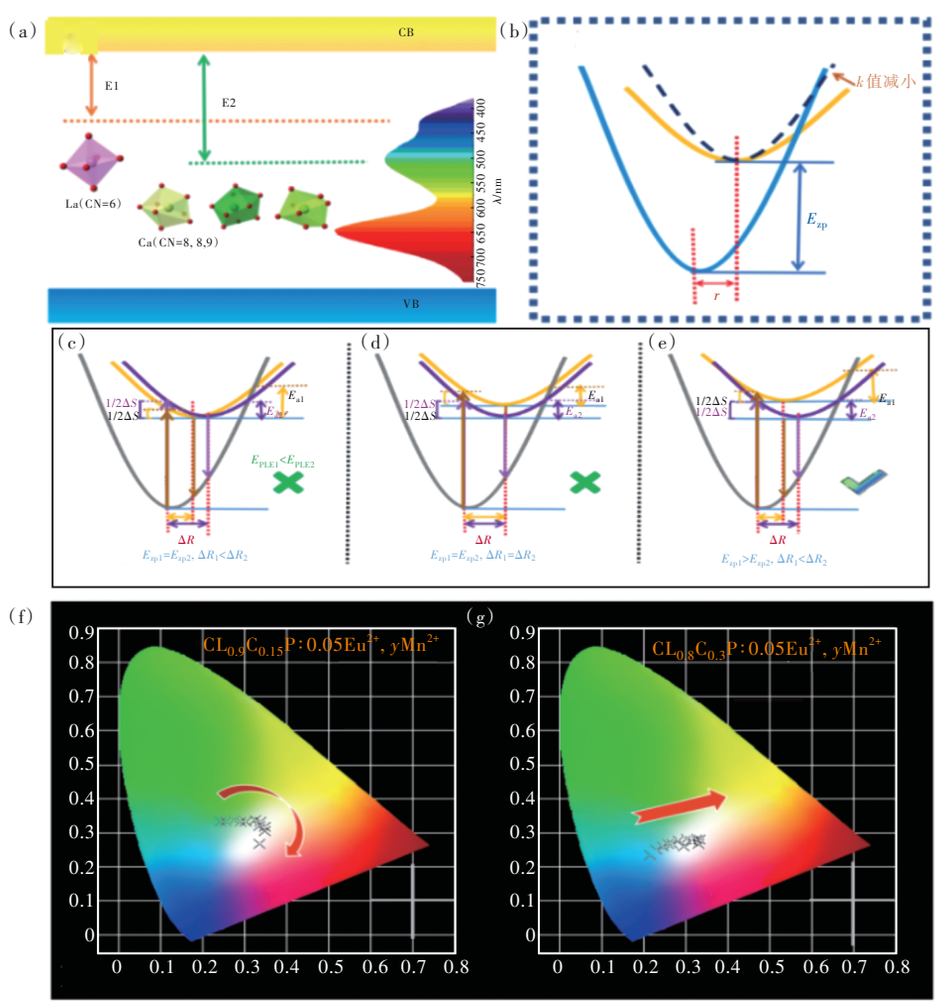

Fig. 5　(a) Schematic diagram of the 5d energy level in the forbidden band. (b) Schematic diagram of configuration. The model diagram only decreases ΔR under different circumstances (c); only E_{zp} enlarges (d); E_{zp} increases, ΔR decreases (e). CIE of $C_9L_{0.9}C_{0.15}P:0.05Eu^{2+},yMn^{2+}$ (f) and $C_9L_{0.8}C_{0.3}P:0.05Eu^{2+},yMn^{2+}$ (g).

the wavelength matching, as shown in Fig. 5(c)-(e). Some of the spectra-relevant data obtained from the actual experiment are listed in Tab. 1 for comparison with Fig. 5(c)-(e) to rule out errors. Data other than E_a in the table can be obtained from Fig. S1, for which the activation energy(E_a) at different locations can be calculated using the Arrhenius equation as follows[29-30]:

$$\ln\left(I_0/I\right) = \ln A - E_a/kT, \tag{7}$$

among them, I_0 and I are the luminous intensities obtained at the temperature of 298 K and other test temperatures, respectively; A is a constant that relates only to the matrix; k is the Boltzmann constant, which has a magnitude of 8.617×10^{-5} eV/K; T is the thermodynamic temperature. When $1/kT$ is used as the abscissa and $\ln(I_0/I)$ is the ordinate, the obtained data are fitted to a straight line, and the slope of the straight line obtained after fitting can be obtained by taking the absolute value. The calculated E_a is 0.105 eV and 0.083 eV, corresponding to shortwave emission and longwave transmission, respectively. It shows that the emission peak at 427 nm has better thermal stability, which is the same as the experimental result.

Tab. 1 The spectral data

	E_a/eV	Emission peak position/nm	Excitation peak position/nm	Stokes displacement/nm
Blue light	0.105	427	300	127
Green light	0.083	510	330	180

Since the corresponding luminous centers of the two emission peaks are in the same matrix, the default mechanical constant k is the same, that is, the curve of the parabola is the same. As can be seen from Fig. 5(c)-(e), when only ΔR decreases, it can conform to the fact that blue light has better temperature stability in the experiment, but the corresponding excitation wavelength is not consistent with the actual situation, so this possibility is excluded. When only E_{zp} increases, Stokes displacement does not change, that is, $\Delta S_1=\Delta S_2$, this possibility is also excluded. Only when E_{zp} increases and R decreases can all data be satisfied. To verify the correctness of the hypothetical model, the changes in ΔR as well as E_{zp} are discussed in the data obtained from experiments. From Fig. 5(c)-(e), it can be seen that the magnitude of E_{zp} depends on the position of the lowest point of the parabola corresponding to the excited state, that is, the equilibrium state. In numerical relationships, $|E_{zp}| \approx |E_{PLE}| - 1/2|\Delta S|$. The blue and green light obtained by using the data in the table correspond to the values of 28 375 and 24 955, respectively. The results show that E_{zp1} greater than E_{zp2}, which is consistent with the statement of E_{zp} in the constructed model.

The offset (ΔR) between the two lowest points of the ground state and the excited state of the two parabolas is related to the degree of rigidity of the crystal lattice. The highly rigid structure corresponds to a small offset. George *et al*. used the Debye temperature(θ_D) to represent the rigidity of the lattice, according to the equation[31-32]:

$$\theta_{D,i} = \sqrt{\frac{3\hbar^2 T N_A}{A_i k_B U_{iso,i}}}, \tag{8}$$

where A_i is the atomic weight of the atom, $\hbar$ is Planck's constant, and k_B is the Boltzmann constant. As can be seen from the formula, the Debye temperature is inversely proportional to the atomic displacement parameter(U_{iso}). Since the data of the two lattice oxygens are the same, the final result is not affected, and the corresponding U_{iso} of Ca1, Ca2, Ca3 and La is 0.018 1, 0.025 2, 0.024 1 and 0.012 2, respectively. The average atomic shift at the six-coordination site (the light-emitting center corresponding to blue light) is the smallest. A smaller U_{iso} corresponds to a higher Debye temperature, which in turn has a smaller ΔR. This result is the same as the $\Delta R1 < \Delta R2$ obtained by the model in Fig. 5(e). From the above discussion, it can be concluded that the different temperature quenching behavior of the two emission peaks is caused by difference in local structure at the two lattices.

In order to prove that the difference in temperature quenching behavior, which does not affect the use of white LEDs, the CIE color coordinates of $C_9L_{0.9}C_{0.15}P:0.05Eu^{2+},yMn^{2+}$ under 330 nm excitation (the corresponding position has been shown in Fig. 5 (f) and (g)) and the corresponding color temperature value are calculated in Tab. S4. As can be seen from the figure, as Mn^{2+} gradually increases, the color coordinate position gradually moves from the high color temperature area to the low color temperature area. And when the concentration of Mn^{2+} reaches 0.3, the ultra-wideband white light emission partially covered by full visible light is realized. Especially when y = 0.35, the color coordinate (0.337, 0.332) of the sample is very close to that of standard white light (0.330, 0.330) and the color temperature (5 239 K) is similar to that of sunlight.

4 Conclusions

In this work, $C_9L_{0.9}C_{0.15}P:0.05Eu^{2+},yMn^{2+}$ and $C_9L_{0.8}C_{0.3}P:0.05Eu^{2+},yMn^{2+}$ were synthesized by high temperature solid state method. The use of XRD matching and refinement methods has shown that the introduction of Mn^{2+} does not change the structure of materials. In the emission spectrum, the emission peak intensity of Eu^{2+} and Mn^{2+} still decreased and increased with the increase of Mn^{2+} concentration, indicating that the energy transfer between Eu^{2+}, Mn^{2+} was not affected by the improvement of the matrix. And this claim is proved by the change of life span. According to Dexter's energy transfer theory and Reisfeld's approximation, the energy transfer mechanism between them is obtained. Among them, there is a dipole-dipole interaction between blue light emitted Eu^{2+} and Mn^{2+}, and the energy transfer mechanism between green light emitted Eu^{2+} and Mn^{2+} is dipole-fourth-order interaction to achieve full visible light coverage. After testing the thermal stability of the sample, it was found that the two different color emission peaks of Eu^{2+} show different temperature quenching behavior. Using the bitmap model, it was concluded that the difference is caused by the difference of the local structure of the two sites, which is proved by the refined data. On the contrary, it can be seen from the CIE color coordinate diagram that when the matrix is $C_9L_{0.9}C_{0.15}P$ and $C_9L_{0.8}C_{0.3}P$, the change from cyan light or green light to white light can be realized by energy transfer. When the concentration of Eu^{2+} is 0.05, the concentration of Mn^{2+} is 0.35 and the matrix is $C_9L_{0.9}C_{0.15}P$, the color coordinate (0.337, 0.332) of the sample is very close to that of standard white light (0.330, 0.330) and the color temperature (5 239 K) is similar to that of sunlight. In addition, the spectral coverage can be covered from 380 nm to 750 nm, so it still has the potential for development in the field of lighting.

Supplementary Information and Response Letter are available for this paper at: http://cjl.lightpublishing.cn/thesisDetails#10.37188/CJL.20230208.

References:

[1] 陈孔岚, 张学亮, 宋恩海, 等. $CaTiF_6\cdot 2H_2O:Mn^{4+}$窄带红色荧光粉的发光性能及其高显指暖白光LED应用[J]. 发光学报, 2023, 44(2): 259-270.
CHEN K L, ZHANG X L, SONG E H, *et al.* Luminescence properties of narrow-band red phosphor $CaTiF_6\cdot 2H_2O:Mn^{4+}$ for warm white light-emitting diodes with high color rendering index [J]. *Chin. J. Lumin.*, 2023, 44(2): 259-270. (in Chinese)

[2] 朱坤领, 游欢欢, 高发明, 等. 窄带型Eu^{2+}掺杂荧光粉理论研究进展[J]. 发光学报, 2022, 43(9): 1405-1412.
ZHU K L, YOU H H, GAO F M, *et al.* Advances in theoretical research on Eu^{2+} doped narrow-band emitting fluorescent materials [J]. *Chin. J. Lumin.*, 2022, 43(9): 1405-1412. (in Chinese)

[3] HAO Z D, ZHANG J H, ZHANG X, *et al.* Phase dependent photoluminescence and energy transfer in $Ca_2P_2O_7:Eu^{2+}$, Mn^{2+} phosphors for white LEDs [J]. *J. Lumin.*, 2008, 128(5-6): 941-944.

[4] SHANG M M, LI G G, GENG D L, *et al.* Blue Emitting $Ca_8La_2(PO_4)_6O_2:Ce^{3+}/Eu^{2+}$ phosphors with high color purity and

brightness for white LED: soft-chemical synthesis, luminescence, and energy transfer properties [J]. *J. Phys. Chem. C*, 2012, 116(18): 10222-10231.

[5] XIE W, MO Y W, ZOU C W, *et al*. Broad color tuning and Eu^{3+}-related photoemission enhancement *via* controllable energy transfer in the $La_2MgGeO_6:Eu^{3+},Bi^{3+}$ phosphor [J]. *Inorg. Chem. Front.*, 2018, 5(5): 1076-1084.

[6] GUO Q F, LIAO L B, MEI L F, *et al*. Color-tunable photoluminescence and energy transfer properties of single-phase $Ba_{10}(PO_4)_6O:Eu^{2+}$, Mn^{2+} phosphors [J]. *J. Solid State Chem.*, 2015, 232: 102-107.

[7] XU H W, WANG L L, QU D, *et al*. Structure and photoluminescence properties of novel $Sr_6Ca_4(PO_4)_6F_2:RE$(*RE*=Eu^{2+}, Mn^{2+}) phosphors with energy transfer for white-emitting LEDs [J]. *RSC Adv.*, 2017, 7(65): 41282-41288.

[8] 吴盼盼, 孟宪国, 许英朝, 等. Sm^{3+}掺杂$NaSr_2Nb_5O_{15}$的新型橙红色荧光粉 [J]. 激光杂志, 2022, 43(8): 37-42.
WU P P, MENG X G, XU Y C, *et al*. Research on new orange-red emitting Sm^{3+}-doped $NaSr_2Nb_5O_{15}$ phosphors [J]. *Laser J.*, 2022, 43(8): 37-42. (in Chinese)

[9] 吕雪杰, 许杰, 林航, 等. Pr^{3+}掺杂红色长余辉发光材料研究进展 [J]. 发光学报, 2022, 43(3): 327-340.
LYU X J, XU J, LIN H, *et al*. Research progress on Pr^{3+} doped red persistent luminescent materials [J]. *Chin. J. Lumin.*, 2022, 43(3): 327-340. (in Chinese)

[10] 宋振, 何丽珠, 刘泉林. Eu^{2+}-Mn^{2+}共掺T相硅酸盐荧光粉的制备与发光性能 [J]. 稀有金属, 2019, 43(11): 1243-1250.
SONG Z, HE L Z, LIU Q L. Synthesis and luminescent properties of Eu^{2+}-Mn^{2+} co-doped T-phase silicate phosphors [J]. *Rare Met.*, 2019, 43(11): 1243-1250. (in Chinese)

[11] 屈冰雁, 王雷. 3d过渡金属离子在无机化合物中的基态能级及变价趋势理论探索 [J]. 发光学报, 2022, 43(12): 1815-1822.
QU B Y, WANG L. Theoretical research on ground state of 3d transition metal ions in inorganic compounds and their charge transition tendencies [J]. *Chin. J. Lumin.*, 2022, 43(12): 1815-1822. (in Chinese)

[12] HUANG C H, CHEN T M. $Ca_9La(PO_4)_7:Eu^{2+},Mn^{2+}$: an emission-tunable phosphor through efficient energy transfer for white light-emitting diodes [J]. *Opt. Express*, 2010, 18(5): 5089-5099.

[13] YU M, LIN J, FANG J. Silica spheres coated with $YVO_4:Eu^{3+}$ layers *via* sol-gel process: A simple method to obtain spherical core-shell phosphors [J]. *Chem. Mater.*, 2005, 17(7): 1783-1791.

[14] LIU X M, LI C X, QUAN Z W, *et al*. Tunable luminescence properties of $CaIn_2O_4:Eu^{3+}$ phosphors [J]. *J. Phys. Chem. C*, 2007, 111(44): 16601-16607.

[15] LIU X M, YAN L S, LIN J. Synthesis and luminescent properties of $LaAlO_3:RE^{3+}$(*RE*=Tm, Tb) nanocrystalline phosphors *via* a sol-gel process [J]. *J. Phys. Chem. C*, 2009, 113(19): 8478-8483.

[16] PAULOSE P I, JOSE G, THOMAS V, *et al*. Sensitized fluorescence of Ce^{3+}/Mn^{2+} system in phosphate glass [J]. *J. Phys. Chem. Solids*, 2003, 64(5): 841-846.

[17] 李凯, 连洪洲, 尚蒙蒙, 等. 稀土发光材料中的能量传递与发光颜色调控 [J]. 中国稀土学报, 2017, 35(1): 19-41.
LI K, LIAN H Z, SHANG M M, *et al*. Recent progress in phosphors with energy transfer for W-LED [J]. *J. Chin. Soc. Rare Earth*, 2017, 35(1): 19-41. (in Chinese)

[18] BLASSE G. Energy transfer in oxidic phosphors [J]. *Phys. Lett. A*, 1968, 28(6): 444-445.

[19] DEXTER D L, SCHULMAN J H. Theory of concentration quenching in inorganic phosphors [J]. *J. Chem. Phys.*, 1954, 22(6): 1063-1070.

[20] GUO N, HUANG Y J, YOU H P, *et al*. $Ca_9Lu(PO_4)_7:Eu^{2+},Mn^{2+}$: A potential single-phased white-light-emitting phosphor suitable for white-light-emitting diodes [J]. *Inorg. Chem.*, 2010, 49(23): 10907-10913.

[21] ANTIPENKO B, BATYAEV I, ERMOLAEV V, *et al*. Radiationless transfer of electron excitation energy between rare earth ions in $POCl_3$-$SnCl_4$ [J]. *Opt. Spektroskop.*, 1970, 29(2): 335.

[22] GENG D L, LI G G, SHANG M M, *et al*. Color tuning *via* energy transfer in $Sr_3In(PO_4)_3:Ce^{3+}/Tb^{3+}/Mn^{2+}$ phosphors [J]. *J. Phys. Chem.*, 2012, 22(28): 14262-14271.

[23] 胡建国, 万国江, 胡学芳, 等. 磷酸钡钙:铈、锰红色荧光粉的研制 [J]. 中国稀土学报, 2005, 23(5): 537-540.
HU J G, WAN G J, HU X F, *et al*. Preparation and characterization of red emiting phosphor $Ba_xCa_{3-x}(PO_4)_2:Ce,Mn$ [J]. *J. Chin. Rare Earth Sci.*, 2005, 23(5): 537-540. (in Chinese)

[24] YANG W J, CHEN T M. Ce^{3+}/Eu^{2+} codoped Ba_2ZnS_3: A blue radiation-converting phosphor for white light-emitting diodes [J]. *Appl. Phys. Lett.*, 2007, 90(17): 171908.

[25] REISFELD R, LIEBLICH-SOFFER N. Energy transfer from UO_2^{2+} to Sm^{3+} in phosphate glass [J]. *J Solid State Chem.*, 1979, 28(3): 391-395.

[26] UEDA J, DORENBOS P, BOS A J J, *et al.* Insight into the thermal quenching mechanism for $Y_3Al_5O_{12}:Ce^{3+}$ through thermoluminescence excitation spectroscopy [J]. *J. Phys. Chem.* C, 2015, 119(44): 25003-25008.

[27] YANG J, ZHANG J W, GAO Z Y, *et al.* Enhanced photoluminescence and thermal stability in solid solution $Ca_{1-x}Sr_xSc_2O_4:Ce^{3+}$ (x=0-1) *via* crystal field regulation and site-preferential occupation [J]. *Inorg. Chem. Front.*, 2019, 6(8): 2004-2013.

[28] BLASSE G, GRABMAIER B C. *Luminescent Materials* [M]. Berlin: Springer, 1994.

[29] HAN J Y, IM W B, KIM D, *et al.* New full-color-emitting phosphor, Eu^{2+}-doped $Na_{2-x}Al_{2-x}Si_xO_4$ ($0\leqslant x\leqslant 1$): obtained using phase transitions for solid-state white lighting [J]. *J. Mater. Chem.*, 2012, 22(12): 5374-5381.

[30] RUAN J, XIE R J, HIROSAKI N, *et al.* Nitrogen gas pressure synthesis and photoluminescent properties of orange-red $SrAlSi_4N_7:Eu^{2+}$ phosphors for white light-emitting diodes [J]. *J. Am. Ceram. Soc.*, 2011, 94(2): 536-542.

[31] GEORGE N C, BIRKEL A, BRGOCH J, *et al.* Average and local structural origins of the optical properties of the nitride phosphor $La_{3-x}Ce_xSi_6N_{11}$ ($0<x\leqslant 3$) [J]. *Inorg. Chem.*, 2013, 52(23): 13730-13741.

[32] GEORGE N G, PELL A J, DANTELLE G, *et al.* Local environments of dilute activator ions in the solid-state lighting phosphor $Y_{3-x}Ce_xAl_5O_{12}$ [J]. *Chem. Mater.*, 2013, 25(20): 3979-3995.

王涛(1984-),男,山东菏泽人,博士,讲师,硕士生导师,2013 年于北京交通大学获得博士学位,主要从事光电材料与器件方面的研究。

E-mail: twang@upc. edu. cn

李盼来(1978-),男,河北河间人,博士,教授,博士生导师,2014 年于北京交通大学获得博士学位,主要从事发光材料及其应用方面的研究。

E-mail: li_panlai@126. com